JACS
JOURNAL OF THE AMERICAN CHEMICAL SOCIETY
Article
pubs.acs.org/JACS

Viewing Human DNA Polymerase β Faithfully and Unfaithfully Bypass an Oxidative Lesion by Time-Dependent Crystallography

Rajan Vyas,[†] Andrew J. Reed,[†,‡] E. John Tokarsky,[†,§] and Zucai Suo*[,†,‡,§]

[†]Department of Chemistry and Biochemistry, [‡]The Ohio State Biochemistry and [§]Biophysics Programs, The Ohio State University, Columbus, Ohio 43210, United States

Supporting Information

ABSTRACT: One common oxidative DNA lesion, 8-oxo-7,8-dihydro-2′-deoxyguanine (8-oxoG), is highly mutagenic in vivo due to its *anti*-conformation forming a Watson−Crick base pair with correct deoxycytidine 5′-triphosphate (dCTP) and its *syn*-conformation forming a Hoogsteen base pair with incorrect deoxyadenosine 5′-triphosphate (dATP). Here, we utilized time-resolved X-ray crystallography to follow 8-oxoG bypass by human DNA polymerase β (hPolβ). In the 12 solved structures, both Watson−Crick (*anti*-8-oxoG:*anti*-dCTP) and Hoogsteen (*syn*-8-oxoG:*anti*-dATP) base pairing were clearly visible and were maintained throughout the chemical reaction. Additionally, a third Mg^{2+} appeared during the process of phosphodiester bond formation and was located between the reacting α- and β-phosphates of the dNTP, suggesting its role in stabilizing reaction intermediates. After phosphodiester bond formation, hPolβ reopened its conformation, pyrophosphate was released, and the newly incorporated primer 3′-terminal nucleotide stacked, rather than base paired, with 8-oxoG. These structures provide the first real-time pictures, to our knowledge, of how a polymerase correctly and incorrectly bypasses a DNA lesion.

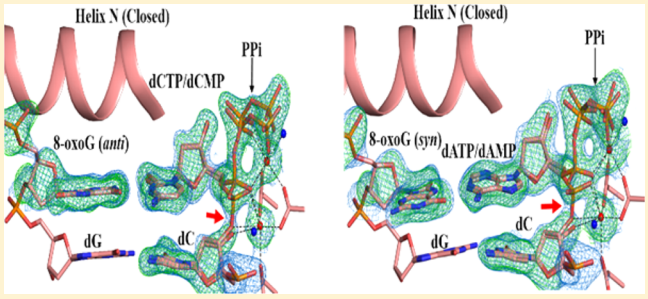

INTRODUCTION

Aerobic respiration, inflammatory responses, phagocytosis, ionizing radiation, pollutants, and xenobiotics generate intracellular reactive oxygen species, which damage genomic DNA and form various oxidative lesions including 8-oxo-7,8-dihydro-2′-deoxyguanine (8-oxoG).[1,2] 8-oxoG lesions can form in genomic double stranded DNA by oxidation of guanine bases or by the incorporation of oxidized guanine nucleotides 8-oxo-7,8-dihydro-2′-deoxyguanine 5′-triphosphate (8-oxoGTP). The incorporation of 8-oxoGTP is minimal due to the action of MTH1, a hydrolase that specifically eliminates oxidized dNTPs and rNTPs.[3] In humans, most 8-oxoG lesions occur in double stranded DNA, where 8-oxoG:dC base pairs are first removed by 8-oxoG DNA glycosylase OGG1, and then repaired by the sequential actions of AP endonuclease 1, human polymerase beta (hPolβ), and DNA ligase I or III/XRCC1 in the base excision repair (BER) pathway (Figure S1A, Supporting Information).[4] For an unrepaired, templating 8-oxoG lesion, its *anti*-conformation forms a Watson−Crick base pair with correct deoxycytidine 5′-triphosphate (dCTP) while its *syn*-conformation forms a Hoogsteen base pair with incorrect deoxyadenosine 5′-triphosphate (dATP). Such incorrect base pairing results in G → T transversion during subsequent rounds of DNA replication (Figure S1A,B). Repair of an 8-oxoG:dA mispair in genomic DNA begins with excision of the undamaged adenine by the adenine DNA glycosylase MYH. The resulting abasic site is then processed similarly by the remaining steps of the BER pathway (Figure S1A).[4] In vivo studies suggest Polβ is the major polymerase involved in this alternative BER pathway, and bypasses 8-oxoG by predominantly inserting either dCTP or dATP.[4,5]

Previous kinetic studies have determined that opposite 8-oxoG, hPolβ incorporates dCTP with a 2-fold, 1×10^4-fold and 2×10^4-fold higher efficiency than dATP, dGTP and dTTP, respectively.[6] Consistent with these data, hPolβ was found to selectively incorporate dCTP over dATP opposite 8-oxoG in a single-nucleotide gapped DNA substrate (8-oxoG-DNA) by ∼2-fold while misincorporation of dGTP and dTTP was barely observable in the presence of catalytic Mg^{2+} (Figure S1D). In contrast, hPolβ was more efficient with mutagenic Mn^{2+}[7] than with Mg^{2+} and incorporated dCTP and dATP onto 8-oxoG-DNA to similar extents (Figure S1D). To reveal a structural basis for the preferential binding of correct dCTP and incorrect dATP, Wilson et al. have used either dideoxy-terminated primers[8] or nonhydrolyzable nucleotide analogs[9] to obtain the crystal structures of the precatalytic ternary complexes of hPolβ with either the *anti*-8-oxoG:*anti*-dCTP Watson−Crick base pair or the *syn*-8-oxoG:*anti*-dATP Hoogsteen base pair in the closed conformations. Although instructive, these structures do not show the process of nucleotide incorporation during 8-oxoG bypass. Recently, Basu and Murakami attempted to catch elusive intermediates formed during bacteriophage N4 RNA polymerase-catalyzed transcription by time-dependent soak-

Received: March 2, 2015
Published: March 31, 2015

DOI: 10.1021/jacs.5b02109
J. Am. Chem. Soc. 2015, 137, 5225−5230

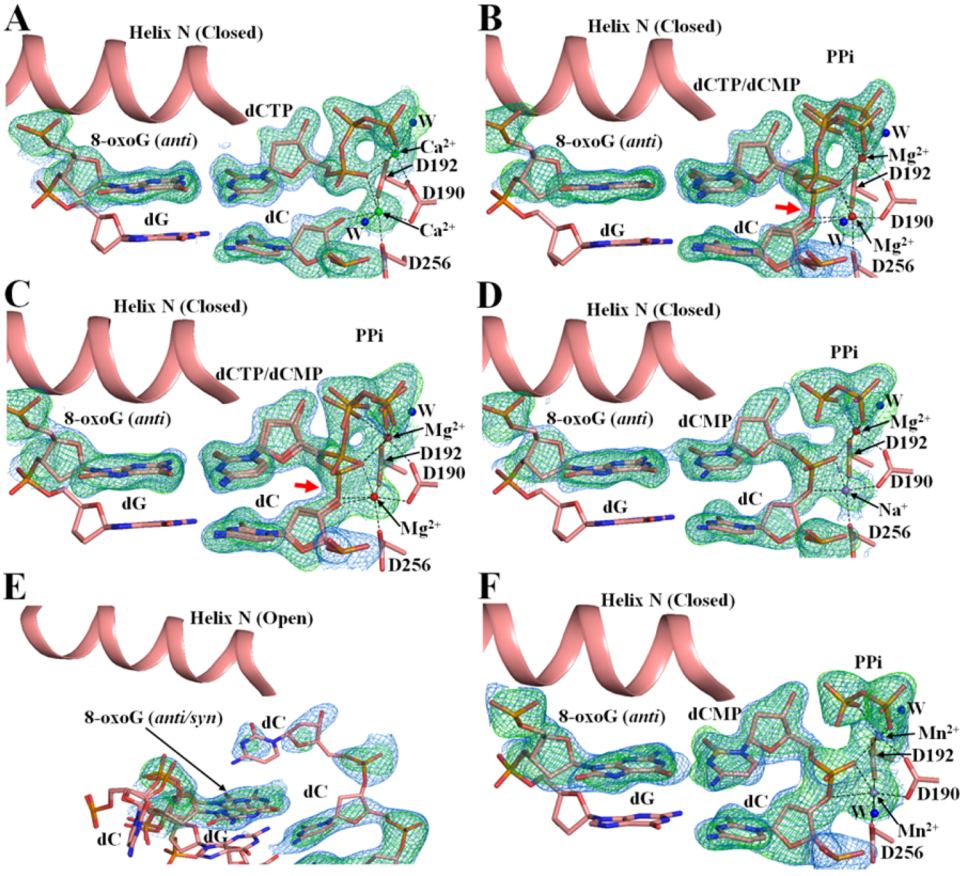

Figure 1. Zoomed active sites to illustrate the binding and time-dependent incorporation of dCTP opposite 8-oxoG by hPolβ. Both $2F_o-F_c$ (blue, 1σ) and F_o-F_c (green, 3σ) maps are shown for the templating 8-oxoG, dCTP or incorporated dCMP, pyrophosphate (PPi), the metal ions at the A-site and B-site, and the primer 3′-terminal nucleotide. Each red arrow indicates the electron density for the newly formed phosphodiester bond. Water molecules (W) are shown as blue spheres. The displayed structures are of the precatalytic ternary complex (A) and those after the precatalytic ternary complex crystals were soaked with either 200 mM Mg^{2+} for 30 s (B), 60 s (C), 80 s (D), and 1 h (E), or with 200 mM Mn^{2+} for 35 s (F). In (E), 8-oxoG was modeled in both *anti*- and *syn*-conformations.

trigger-freeze X-ray crystallography.[10] Similarly, Yang et al. developed a time-resolved crystallization method capable of capturing structural snapshots at specific time points of phosphodiester bond formation during correct nucleotide incorporation onto undamaged DNA by human DNA polymerase η (hPolη).[11] Their methods were adapted by Wilson et al. to capture several structural intermediates formed in the processes of nucleotide incorporation onto undamaged DNA by hPolβ.[12] Here, we employed a similar time-resolved crystallization method to structurally visualize the bypass of a DNA lesion for the first time, to our knowledge.

EXPERIMENTAL SECTION

Preparation of Protein and DNA. Human DNA polymerase β (hPolβ) was overexpressed and purified as reported earlier.[6] After purification, the protein was washed four times with several volumes of the 20 mM Bis-Tris (pH 7.0) buffer, concentrated to 15 mg/mL and stored at −80 °C. The single-nucleotide gapped DNA substrate 8-oxoG-DNA (Figure S1C, 1 mM) was prepared by mixing equimolars of a 16-mer template (5′-CCGACG$_o$GCGCATCAGC-3′), where G_o represents 8-oxoG, a 10-mer upstream primer (5′-GCTGATGCGC-3′) and a 5′-phosphorylated 5-mer downstream primer (5′-P-GTCGG-3′) and heating to 80 °C and then cooling to room temperature.

Crystallization and Structure Determination. To form the binary complex of hPolβ and a single-nucleotide gapped DNA substrate, the purified protein (15 mg/mL) and 8-oxoG-DNA (1 mM) were mixed in a 1:1 volume ratio. The resulting mixture was then heated to 40 °C and then slowly cooled to room temperature as reported previously.[8] The binary complex crystals were obtained using the hanging drop vapor diffusion method by equilibrating against a reservoir buffer containing 50 mM imidazole (pH 7.5), 16−18% PEG3350, and 350 mM sodium acetate[8] at room temperature and streak seeded after 24 h. To form the precatalytic ternary complex crystal, the binary complex crystals were transferred to a cryosolution containing 50 mM imidazole (pH 7.5), 16−18% PEG3350, 90 mM sodium acetate, 15% ethylene glycol, 50 mM $CaCl_2$ and an incoming nucleotide (dCTP or dATP). The precatalytic ternary crystals were flash-frozen in liquid N_2. To initiate nucleotide incorporation reaction in the crystals, the precatalytic ternary complex crystals were transferred to another cryosolution containing 50 mM imidazole (pH 7.5), 16−18% PEG3350, 90 mM sodium acetate, 15% ethylene glycol, and 200 mM $MgCl_2$ or $MnCl_2$, and soaked for various times. The reactions were stopped by flash freezing the crystals in liquid N_2. X-ray diffraction data were collected using LRL-CAT beamline facilities at Advance Photon Source (APS), Argonne National Laboratory. The X-ray diffraction data were processed using MOSFLM.[13] The structures were solved through the molecular replacement method by PHASER[14] using a previously determined structure (PDB code: 4KLD)[12] as the initial model in the absence of ligands and solvent molecules. Initial models for all structures were generated by performing simulated annealing using Phenix.[15] Further iterations of refinement were carried out using REFMAC5.[16] COOT[17] was used for visualization and model building. Quality of the models was assessed using PROCHECK.[18] All electron density omit maps were generated using Phenix.[15] Figures were created using PYMOL.[19]

DOI: 10.1021/jacs.5b02109
J. Am. Chem. Soc. 2015, 137, 5225−5230

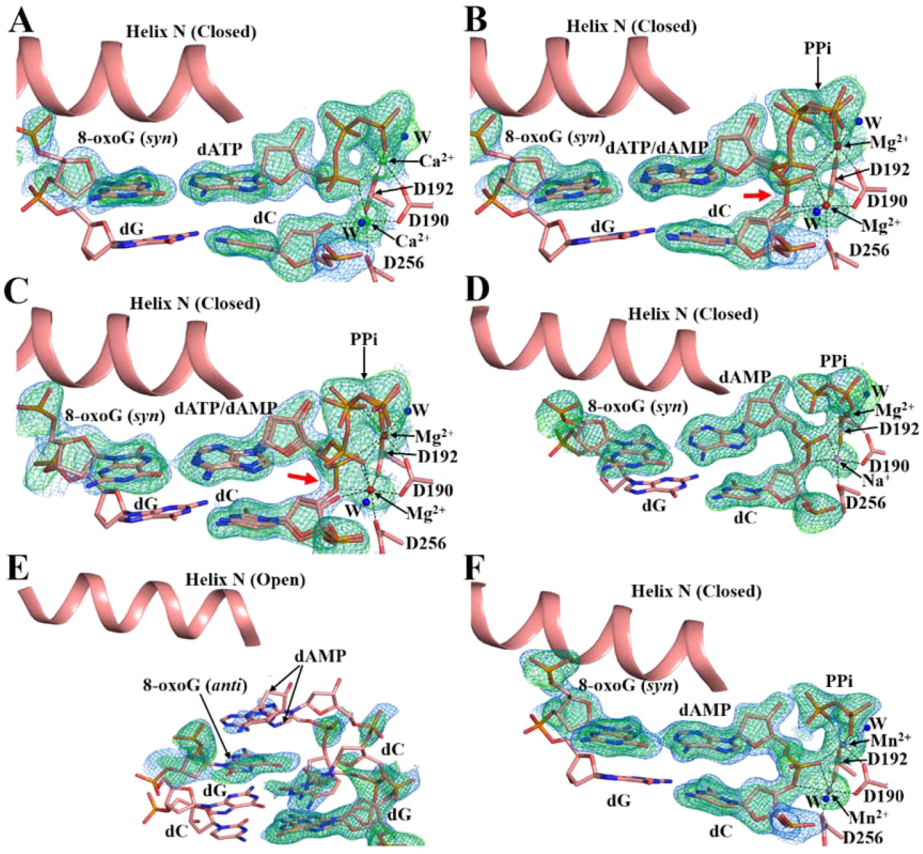

Figure 2. Zoomed active sites to illustrate the binding and time-dependent incorporation of dATP opposite 8-oxoG by hPolβ. Both $2F_o-F_c$ (blue, 1σ) and F_o-F_c (green, 3σ) maps are shown for the templating 8-oxoG, dATP or incorporated dAMP, PPi, the metal ions at the A-site and B-site, and the primer 3′-terminal nucleotide. Each red arrow indicates the electron density for the newly formed phosphodiester bond. Water molecules are shown as blue spheres. The displayed structures are of the precatalytic ternary complex (A) and those after the precatalytic ternary complex crystals were soaked with either 200 mM Mg^{2+} for 30 s (B), 60 s (C), 80 s (D), and 1 h (E), or with 200 mM Mn^{2+} for 35 s (F). In (E), the last three nucleotides at the primer 3′-terminus were modeled in two different conformations.

^{32}P-Labeled Primer Extension Assay. A preincubated solution of hPolβ (10 nM) and 5′-[^{32}P]-labeled 8-oxoG-DNA (30 nM) was reacted for 15 s with a dNTP (100 μM) in the buffer (50 mM Tris-HCl (pH 7.8 at 25 °C), 5 mM $MgCl_2$ or $MnCl_2$, 50 mM NaCl, 0.1 mM EDTA, 5 mM DTT, 10% glycerol, and 0.1 mg/mL of BSA) at 25 °C. The reaction was quenched with 0.37 M EDTA. Reaction products were resolved using sequencing gel electrophoresis (17% (w/v) acrylamide, 8 M urea).

Atomic coordinates have been deposited in the Protein Data Bank under the following accession codes: 4RPX (dCTP, precatalytic, Ca^{2+}), 4RPY (dCTP, 30 s, Mg^{2+}), 4RPZ (dCTP, 60 s, Mg^{2+}), 4RQ0 (dCTP, 80 s, Mg^{2+}), 4RQ1 (dCTP, 1 h, Mg^{2+}), 4RQ2 (dCTP, 35 s, Mn^{2+}), 4RQ3 (dATP, precatalytic, Ca^{2+}), 4RQ4 (dATP, 30 s, Mg^{2+}), 4RQ5 (dATP, 60 s, Mg^{2+}), 4RQ6 (dATP, 80 s, Mg^{2+}), 4RQ7 (dATP, 1 h, Mg^{2+}), and 4RQ8 (dATP, 35 s, Mn^{2+}).

RESULTS AND DISCUSSION

Precatalytic Ternary Structures. The binary complex of hPolβ and 8-oxoG-DNA (hPolβ·8-oxoG-DNA) was first crystallized and the resulting crystals were then soaked with a cryosolution containing noncatalytic Ca^{2+} and either dCTP or dATP in order to form precatalytic ternary complex crystals. The precatalytic ternary complex crystals of hPolβ·8-oxoG-DNA·dATP (Table S2) and hPolβ·8-oxoG-DNA·dCTP (Table S1) diffracted to 2.00 and 1.90 Å, respectively, and their structures were solved through molecular replacement. Both F_o-F_c and $2F_o-F_c$ electron density maps of the precatalytic ternary structures clearly show the closed conformation of hPolβ relative to the open binary structure of hPolβ·8-oxoG-DNA as seen previously with undamaged DNA.[12] Also visible are the *anti*-8-oxoG:*anti*-dCTP Watson−Crick or *syn*-8-oxoG:*anti*-dATP Hoogsteen base pairing and two hexacoordinated Ca^{2+} ions at the A-site and B-site, liganded by the primer 3′-OH, the triphosphate of dCTP or dATP, water, and the carboxylates of D190, D192, and D256 (Figures 1A, 2A, and S2). The precatalytic structures of hPolβ·8-oxoG-DNA·dCTP and hPolβ·8-oxoG-DNA·dATP are nearly superimposable with an RMSD of 0.30 Å and only a slight repositioning of the nascent base pair (Figure S2A). Notably, other than the Hoogsteen base pairing, the *syn*-conformation of 8-oxoG is further stabilized by a hydrogen bond (2.8 Å) between the O8 atom and the side chain of R283 in Helix N, which occupies the minor groove (Figure S2H). The Ca^{2+} ions were positioned at the same A-site and B-site as the two Mg^{2+} ions in the precatalytic ternary structures of hPolβ[9] and other polymerases.[20−29]

Reaction-State Structures. To trigger phosphodiester bond formation, the precatalytic hPolβ·8-oxoG-DNA·dCTP and hPolβ·8-oxoG-DNA·dATP crystals were transferred to a cryosolution containing 200 mM catalytic Mg^{2+} to initiate the exchange with noncatalytic Ca^{2+} ions at the A-site and B-site of hPolβ. The reaction was stopped after 30, 60, and 80 s by flash freezing the crystals in liquid nitrogen. The crystals diffracted to 1.90−2.20 Å for the dCTP reaction intermediates (Table S1) and 2.10−2.32 Å for the dATP reaction intermediates (Table

DOI: 10.1021/jacs.5b02109
J. Am. Chem. Soc. 2015, 137, 5225−5230

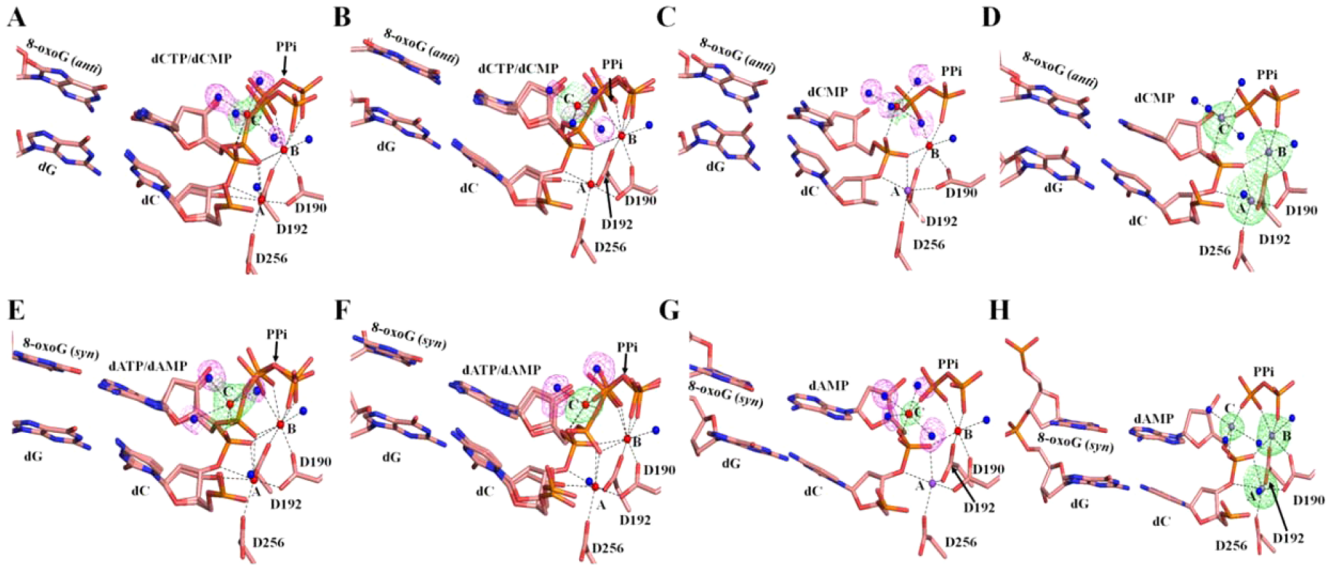

Figure 3. Three divalent metal ion binding sites at the active site of hPolβ during dCTP or dATP incorporation opposite 8-oxoG. After the crystals of the precatalytic ternary complexes of hPolβ·8-oxoG-DNA·dCTP and hPolβ·8-oxoG-DNA·dATP were soaked with Mg^{2+} for 30, 60, and 80 s, dCTP incorporation had completed by 50% (A), 80% (B) and 100% (C), respectively, while dATP incorporation had finished by 30% (E), 70% (F) and 100% (G), respectively. When the crystals of the precatalytic ternary complexes of hPolβ·8-oxoG-DNA·dCTP and hPolβ·8-oxoG-DNA·dATP were soaked with Mn^{2+} for 35 s, both dCTP (D) and dATP (H) were 100% incorporated. For panels (A−C) and (E−G), the F_o-F_c omit maps were contoured at 3σ to show the electron density (green) of Mg^{2+} at the C-site and the electron density (pink) for associated water molecule ligands. The F_o-F_c omit maps contoured at 5σ show the electron densities (green) of the three Mn^{2+} ions after dCTP (D) and dATP (H) incorporation. The side chains of the aspartate residues at the active site are shown as stick models while the water molecule ligands (blue) and the metal ions of Mg^{2+} (red), Mn^{2+} (gray), and Na^{+} (purple) are denoted as spheres. For description of coordinating ligands and distances, please see Table S3.

S2) and the structures were solved by molecular replacement. The structures after 30 and 60 s metal ion-exchange, partial occupancies of the reactants (primer 3′-nucleotide and dCTP or dATP) and products (pyrophosphate and dCMP or dAMP) were modeled to account for the observed electron density gain associated with phosphodiester bond formation between the primer 3′-OH and the α-phosphate (Pα) of dNTP, and electron density loss associated with bond breakage between the α- and β-phosphates of the dNTP (Figure S3). Using this approach, both F_o-F_c and $2F_o-F_c$ electron density maps for 30 and 60 s metal ion-exchange were appropriately modeled at 50 and 80% dCTP incorporation and 30 and 70% dATP misincorporation, respectively (Figure S3). For partial dCTP incorporation, the primer 3′-OH moved 0.8−1.1 Å upward relative to its position in the precatalytic state structures and launched the in-line nucleophilic attack on Pα, leading to 1.0 Å downward movement of Pα and the steric inversion of its nonbridging oxygens (Figure 1B,C). Similarly, for partial dATP incorporation, the primer 3′-OH and Pα moved toward each other by 0.9−1.3 Å and 1.0−1.1 Å, respectively (Figure 2B,C). Surprisingly, besides the two typical hexacoordinated Mg^{2+} ions at the A-site and B-site as observed in the precatalytic ternary structures of other polymerases,[20−29] additional electron density near Pα and Pβ was observed (Figure 3) and modeled as a third Mg^{2+} at 0.5−0.8 occupancy (Tables S1 and S2). This C-site Mg^{2+} was liganded by the nonbridging oxygen atoms of Pα and Pβ and water molecules (Figure 3 and Table S3).

Postcatalytic Ternary Structures. In comparison, the structures after 80 s metal ion-exchange display 100% phosphodiester bond formation and no electron density between Pα and Pβ of either dCTP (Figure 1D) or dATP (Figure 2D), indicating the nucleotide incorporation was slower in the crystals than in solution (Figure S1D). The slower rate was possibly caused by decreased thermal motion in crystallo and by the viscous cryosolution.[11,12] Furthermore, the F_o-F_c omit maps contoured at 3σ show the presence of the C-site ion which was modeled as Mg^{2+} at full occupancy (Figure 3C−G). Although the B-site Mg^{2+} persisted, the A-site ion was modeled as Na^{+} based on the number of coordinating ligands and their distances from the ion[12] (Figure S4A,B). Such Mg^{2+} to Na^{+} exchange presumably facilitated the subsequent closed to open protein conformational change and pyrophosphate release.

Appearance of the Third Divalent Metal Ion at the Active Site. To provide additional evidence for the existence of the C-site ion, the precatalytic crystals of hPolβ·8-oxoG-DNA·dCTP and hPolβ·8-oxoG-DNA·dATP were soaked with 200 mM Mn^{2+} to exchange for Ca^{2+} for 35 s to initiate nucleotide incorporation. The resulting crystals diffracted to 2.2 (Table S1) and 2.0 Å (Table S2), respectively. In the refined structures (Figures 1F and 2F), the F_o-F_c and $2F_o-F_c$ electron density maps clearly show 100% product formation and two hexacoordinated Mn^{2+} at the A-site and B-site. The presence of the C-site Mn^{2+} in both structures is validated by the F_o-F_c electron density map contoured at 5σ, and this Mn^{2+} is coordinated by water molecules and nonbridging oxygen atoms of the newly formed phosphodiester bond and pyrophosphate (Figure 3D−H and Table S3). Moreover, overlaying the product-state structures from 80 s Ca^{2+} to $Mg^{2+}$and 35 s Ca^{2+} to Mn^{2+} ion-exchange shows the divalent metal ions at each site were nearly superimposable (Figure S4C,D). Previously, with undamaged DNA and correct dNTP, the third Mg^{2+} was observed in both the reaction-state and product-state structures with hPolη,[11] but only in the product-state structure with hPolβ.[12] More recently during submission of this manuscript, Wilson et al. published a study to show a third divalent metal ion in the precatalytic, reaction-state, and postcatalytic structures for *anti*-8-oxoGTP incorporation opposite cytosine

DOI: 10.1021/jacs.5b02109
J. Am. Chem. Soc. 2015, 137, 5225−5230

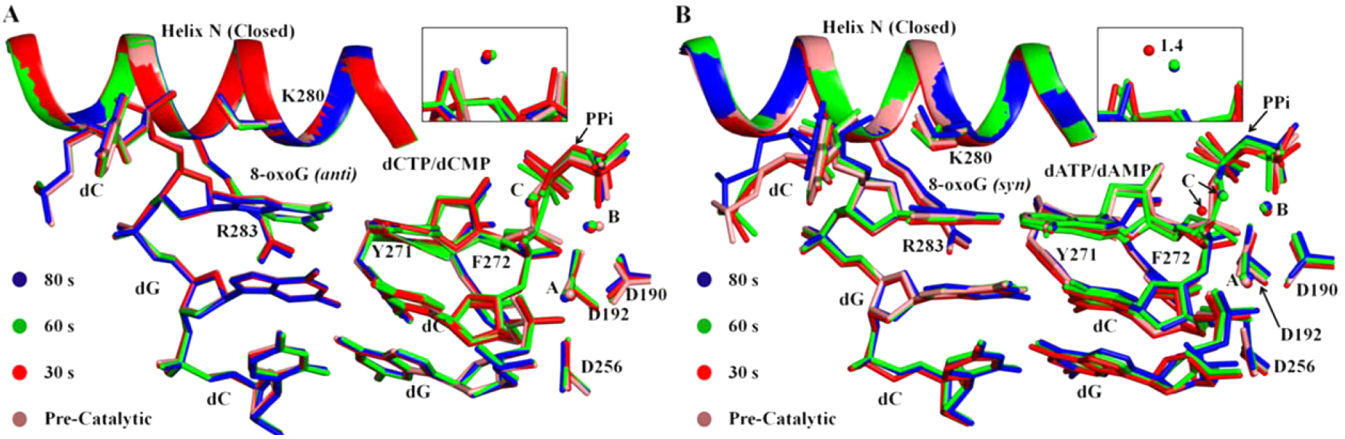

Figure 4. Zoomed active sites in the ternary complexes with either Ca^{2+} or Mg^{2+} at the A-, B-, and C-site. Superposition of the precatalytic (Ca^{2+}) ternary structure of hPolβ·8-oxoG-DNA·dCTP (A) or hPolβ·8-oxoG-DNA·dATP (B) with its corresponding structures after soaking the precatalytic ternary complex crystals with Mg^{2+} for 30, 60, and 80 s shows the differences at the active site of hPolβ. The three metal ion sites are marked as A, B and C and shown as spheres. The RMSD values for the hPolβ backbone in the 30, 60, and 80 s structures relative to the precatalytic complex structure are 0.13, 0.17, and 0.25 Å in (A), and 0.14, 0.29, and 0.49 Å in (B). The close-up views show the location of the C-site metal ion at a different angle. In (A), the C-site metal ion is at the same position. In contrast, the C-site metal ion in (B) moved 1.4 Å from its position in the 30 s structure (red sphere) to its position in the 60 (green sphere) and 80 s (blue sphere) structures.

and only in the postcatalytic structure for *syn*-8-oxoGTP incorporation opposite adenine.[30] This is the first instance, to our knowledge, of a precatalytic structure containing a third divalent metal ion but is likely unique to the 8-oxoGTP substrate as its O8 position stabilizes two bridging water molecules which act as coordinating ligands for this third metal ion.[30] Together, these previous and our current time-resolved crystallization studies strongly suggest that DNA polymerases likely use a "three-metal-ion mechanism" for catalysis,[11] rather than the "two-metal-ion mechanism" proposed by L. Beese and T. Steitz,[31] which is based on *Escherichia coli* DNA polymerase I and has been supported by numerous precatalytic ternary structures of other polymerases.[20,21,32−35] The potential role of the C-site Mg^{2+} is to neutralize the negative charge in the transition state and facilitate phosphodiester bond formation.[11] Notably, the number of ligands for the C-site ion varied from four to six due to different numbers of water ligands (Figure 3), which is likely caused by the labile nature of the water ligands.

Comparison of the Precatalytic, Reaction-State and Postcatalytic Ternary Structures. Interestingly, overlaying the structures of the precatalytic ternary complex with the reaction-state and postcatalytic ternary complexes after metal ion-exchange for 30, 60, and 80 s (Figure 4) indicates that the *anti*-8-oxoG:*anti*-dC Watson−Crick and *syn*-8-oxoG:*anti*-dA Hoogsteen base pairing were maintained throughout the chemistry step. In addition, all structures of hPolβ were in the closed conformation and nearly superimposable with RMSDs of 0.13−0.49 Å. Other than the primer 3′-nucleotide and incoming nucleotide involved in product formation described above, the DNA substrate and the active site residues barely changed their positions. Notably, among the three metal ions, only the C-site ion substantially altered its position (1.4 Å) during dATP incorporation (Figure 4B), indicating its dynamic nature. Failure to observe this notable change in the C-site ion position during correct incorporation by both hPolβ (Figure 4A) and hPolη[11] is possibly due to the inability to capture earlier reaction-state structures.

Postcatalytic Binary Structures. To monitor changes in the product-state structure caused by pyrophosphate release, the precatalytic crystals of hPolβ·8-oxoG-DNA·dCTP and hPolβ·8-oxoG-DNA·dATP were soaked with $MgCl_2$ for longer than 80 s and several structures were solved. However, only the 1 h structures of 2.70 (Table S1) and 2.00 Å (Table S2) for dCTP and dATP incorporation, respectively, show significant differences from the corresponding 80 s structures (Figures 1D and 2D). In the 1 h postcatalytic binary structures, both pyrophosphate and the three metal ions had dissociated, and hPolβ had transitioned from closed to open conformation as indicated by the movement of Helix N away from the active site, and the repositioning of the active site residues Y271, F272, D192, D190 and D256 (Figures 1E, 2E and S5). Such postcatalytic active site rearrangement and protein conformational change are consistent with those projected through kinetic studies.[36−39] The pyrophosphate dissociation from the crystals observed here was not seen previously after correct nucleotide incorporation onto undamaged DNA by hPolβ in crystallo.[12] Furthermore, 8-oxoG in the nicked DNA product after dCTP incorporation was best modeled in both *anti*- and *syn*-conformations (Figure S6A), and the incorporated dCMP had poor electron density and stacked, rather than base paired, with 8-oxoG (Figure 1E). Similarly, in the postcatalytic binary product structure after dATP incorporation (Figure 2E), 8-oxoG was better modeled in the *anti*-conformation (Figure S6B) and stacked with the incorporated dAMP. Moreover, there were two separate electron densities for the phosphate portion of dAMP, leading to the modeling of alternative conformations for the last three nucleotides of the primer 3′-terminus (Figure 2E). These base-stacking patterns after dCTP and dATP incorporation are not suitable for further DNA synthesis and thereby may facilitate the transition from the closed to open conformation of hPolβ. Alternatively, following nucleotide incorporation, hPolβ may first transition from the closed to the open binary conformation, allowing the observed stacking interactions to occur. Either mechanism would prevent further upstream primer elongation and downstream primer displacement.

■ CONCLUSIONS

In summary, our time-resolved crystallization studies have revealed that both Watson−Crick (*anti*-8-oxoG:*anti*-dCTP)

DOI: 10.1021/jacs.5b02109
J. Am. Chem. Soc. 2015, 137, 5225−5230

and Hoogsteen (*syn*-8-oxoG:*anti*-dATP) base pairing modes were persistent throughout phosphodiester bond formation. This bond formation was facilitated by a third divalent metal ion that has never been observed in any precatalytic ternary structure of a polymerase. Transition from the closed ternary to open binary conformation was facilitated by the stacking interactions between the incorporated nucleotide (dAMP or dCMP) and the templating 8-oxoG, suggesting that the open binary conformation is primed for the transfer of the nicked DNA substrate to a DNA ligase for continuous BER. Through the snapshots of nucleotide incorporation obtained by time-resolved crystallography, this study provides structural details important for the understanding of error-free and error-prone DNA lesion bypass.

■ ASSOCIATED CONTENT

Supporting Information

Supplemental figures and crystallographic data tables. This material is available free of charge via the Internet at http://pubs.acs.org.

■ AUTHOR INFORMATION

Corresponding Author

*suo.3@osu.edu

Notes

The authors declare no competing financial interest.

■ ACKNOWLEDGMENTS

This work was supported by National Institutes of Health grants (ES009127, ES024585) and National Science Foundation grant (MCB-0960961) to Z.S. The authors are grateful for the usage of the Advanced Photon Source, an Office of Science User Facility operated for the U.S. Department of Energy (DOE) Office of Science by Argonne National Laboratory, which was supported by the U.S. DOE under Contract No. DE-AC02-06CH11357. The authors are also grateful for the usage of the Lilly Research Laboratories Collaborative Access Team (LRL-CAT) beamline at Sector 31 of the Advanced Photon Source provided by Eli Lilly Company, which operates the facility.

■ REFERENCES

(1) Cooke, M. S.; Evans, M. D.; Dizdaroglu, M.; Lunec, J. *FASEB J.* **2003**, *17*, 1195.
(2) Asami, S.; Hirano, T.; Yamaguchi, R.; Tomioka, Y.; Itoh, H.; Kasai, H. *Cancer Res.* **1996**, *56*, 2546.
(3) Nakabeppu, Y.; Kajitani, K.; Sakamoto, K.; Yamaguchi, H.; Tsuchimoto, D. *DNA Repair* **2006**, *5*, 761.
(4) Beard, W. A.; Batra, V. K.; Wilson, S. H. *Mutat. Res.* **2010**, *703*, 18.
(5) Cabelof, D. C.; Raffoul, J. J.; Yanamadala, S.; Guo, Z.; Heydari, A. R. *Carcinogenesis* **2002**, *23*, 1419.
(6) Brown, J. A.; Duym, W. W.; Fowler, J. D.; Suo, Z. *J. Mol. Biol.* **2007**, *367*, 1258.
(7) Pelletier, H.; Sawaya, M. R.; Wolfle, W.; Wilson, S. H.; Kraut, J. *Biochemistry* **1996**, *35*, 12762.
(8) Krahn, J. M.; Beard, W. A.; Miller, H.; Grollman, A. P.; Wilson, S. H. *Structure* **2003**, *11*, 121.
(9) Batra, V. K.; Shock, D. D.; Beard, W. A.; McKenna, C. E.; Wilson, S. H. *Proc. Natl. Acad. Sci. U. S. A.* **2012**, *109*, 113.
(10) Basu, R. S.; Murakami, K. S. *J. Biol. Chem.* **2013**, *288*, 3305.
(11) Nakamura, T.; Zhao, Y.; Yamagata, Y.; Hua, Y. J.; Yang, W. *Nature* **2012**, *487*, 196.
(12) Freudenthal, B. D.; Beard, W. A.; Shock, D. D.; Wilson, S. H. *Cell* **2013**, *154*, 157.
(13) Battye, T. G.; Kontogiannis, L.; Johnson, O.; Powell, H. R.; Leslie, A. G. *Acta Crystallogr., Sect. D: Biol. Crystallogr.* **2011**, *67*, 271.
(14) McCoy, A. J.; Grosse-Kunstleve, R. W.; Adams, P. D.; Winn, M. D.; Storoni, L. C.; Read, R. J. *J. Appl. Crystallogr.* **2007**, *40*, 658.
(15) Adams, P. D.; Afonine, P. V.; Bunkoczi, G.; Chen, V. B.; Davis, I. W.; Echols, N.; Headd, J. J.; Hung, L. W.; Kapral, G. J.; Grosse-Kunstleve, R. W.; McCoy, A. J.; Moriarty, N. W.; Oeffner, R.; Read, R. J.; Richardson, D. C.; Richardson, J. S.; Terwilliger, T. C.; Zwart, P. H. *Acta Crystallogr., Sect. D: Biol. Crystallogr.* **2010**, *66*, 213.
(16) Murshudov, G. N.; Skubak, P.; Lebedev, A. A.; Pannu, N. S.; Steiner, R. A.; Nicholls, R. A.; Winn, M. D.; Long, F.; Vagin, A. A. *Acta Crystallogr., Sect. D: Biol. Crystallogr.* **2011**, *67*, 355.
(17) Emsley, P.; Cowtan, K. *Acta Crystallogr., Sect. D: Biol. Crystallogr.* **2004**, *60*, 2126.
(18) Laskowski, R. A.; Rullmannn, J. A.; MacArthur, M. W.; Kaptein, R.; Thornton, J. M. *J. Biomol. NMR* **1996**, *8*, 477.
(19) DeLano, W. L. *PYMOL*; DeLano Scientific: San Carlos, CA, 2002.
(20) Steitz, T. A. *Nature* **1998**, *391*, 231.
(21) Doublie, S.; Tabor, S.; Long, A. M.; Richardson, C. C.; Ellenberger, T. *Nature* **1998**, *391*, 251.
(22) Li, Y.; Korolev, S.; Waksman, G. *EMBO J.* **1998**, *17*, 7514.
(23) Rodriguez, A. C.; Park, H. W.; Mao, C.; Beese, L. S. *J. Mol. Biol.* **2000**, *299*, 447.
(24) Garcia-Diaz, M.; Bebenek, K.; Krahn, J. M.; Pedersen, L. C.; Kunkel, T. A. *DNA Repair* **2007**, *6*, 1333.
(25) Ding, J.; Das, K.; Hsiou, Y.; Sarafianos, S. G.; Clark, A. D., Jr.; Jacobo-Molina, A.; Tantillo, C.; Hughes, S. H.; Arnold, E. *J. Mol. Biol.* **1998**, *284*, 1095.
(26) Vaisman, A.; Ling, H.; Woodgate, R.; Yang, W. *EMBO J.* **2005**, *24*, 2957.
(27) Alt, A.; Lammens, K.; Chiocchini, C.; Lammens, A.; Pieck, J. C.; Kuch, D.; Hopfner, K. P.; Carell, T. *Science* **2007**, *318*, 967.
(28) Yang, W. *Nat. Struct. Mol. Biol.* **2008**, *15*, 1228.
(29) Silverstein, T. D.; Jain, R.; Johnson, R. E.; Prakash, L.; Prakash, S.; Aggarwal, A. K. *Structure* **2010**, *18*, 1463.
(30) Freudenthal, B. D.; Beard, W. A.; Perera, L.; Shock, D. D.; Kim, T.; Schlick, T.; Wilson, S. H. *Nature* **2015**, *517*, 635.
(31) Beese, L. S.; Steitz, T. A. *EMBO J.* **1991**, *10*, 25.
(32) Kiefer, J. R.; Mao, C.; Braman, J. C.; Beese, L. S. *Nature* **1998**, *391*, 304.
(33) Wang, J.; Sattar, A. K.; Wang, C. C.; Karam, J. D.; Konigsberg, W. H.; Steitz, T. A. *Cell* **1997**, *89*, 1087.
(34) Kohlstaedt, L. A.; Wang, J.; Friedman, J. M.; Rice, P. A.; Steitz, T. A. *Science* **1992**, *256*, 1783.
(35) Pelletier, H.; Sawaya, M. R.; Kumar, A.; Wilson, S. H.; Kraut, J. *Science* **1994**, *264*, 1891.
(36) Xu, C.; Maxwell, B. A.; Brown, J. A.; Zhang, L.; Suo, Z. *PLoS Biol.* **2009**, *7*, e1000225.
(37) Joyce, C. M.; Benkovic, S. J. *Biochemistry* **2004**, *43*, 14317.
(38) Showalter, A. K.; Tsai, M. D. *Biochemistry* **2002**, *41*, 10571.
(39) Towle-Weicksel, J. B.; Dalal, S.; Sohl, C. D.; Doublie, S.; Anderson, K. S.; Sweasy, J. B. *J. Biol. Chem.* **2014**, *289*, 16541.

DOI: 10.1021/jacs.5b02109
J. Am. Chem. Soc. 2015, 137, 5225−5230